Curr Radiol Rep (2015) 3:7
DOI 10.1007/s40134-015-0088-x

CT Liver Imaging: What is New?

Nicolaus A. Wagner-Bartak · Aran M. Toshav · Eric P. Tamm · Ott Le · Sheela Agarwal · Chaan Ng · Aliya Qayyum

Published online: 6 February 2015

Abstract This review article aims to bring the reader up to date on advances in liver CT imaging, with an emphasis on the literature from the past year. Recent studies and developments in hepatic imaging using dual-energy CT, perfusion CT, low-tube-voltage imaging, and iterative reconstruction techniques are discussed.

This article is part of the Topical Collection on *Abdominal CT-An Update on Applications and New Developments*.

N. A. Wagner-Bartak (✉) · E. P. Tamm · O. Le · C. Ng · A. Qayyum
Division of Diagnostic Imaging, Department of Diagnostic Radiology, The University of Texas MD Anderson Cancer Center, 1515 Holcombe Blvd, Houston, TX 77030, USA
e-mail: nwagner@mdanderson.org

E. P. Tamm
e-mail: etamm@mdanderson.org

O. Le
e-mail: ott.le@mdanderson.org

C. Ng
e-mail: cng@mdanderson.org

A. Qayyum
e-mail: aqayyum@mdanderson.org

A. M. Toshav
LSUHSC New Orleans, 1542 Tulane Ave, New Orleans, LA 70112, USA
e-mail: atosha@lsuhsc.edu

S. Agarwal
Division of Abdominal Imaging and Intervention, Department of Radiology, Massachusetts General Hospital, 55 Fruit Street, Wht 2-270, Boston, MA 02114, USA
e-mail: sagarwal5@partners.org

Keywords Liver CT · Dual-energy CT · Perfusion CT · Low-tube-voltage · Iterative reconstruction · Hepatocellular carcinoma

Introduction

CT imaging of the liver continues to evolve. Dual-energy CT (DECT), the acquisition of imaging information at more than one X-ray energy level, has been shown to improve the detection of hypervascular and hypovascular focal liver lesions, including metastases and HCC, and shows promise for the assessment of hepatic iron accumulation and hepatic steatosis [1, 2•, 3, 4]. Development of high amperage X-ray tubes has allowed for imaging at lower kilovoltage settings, increasing the conspicuity of hypervascular liver lesions while saving radiation dose when performed in appropriately selected, small-to-medium-sized adults. Perfusion CT is being investigated as a potential imaging biomarker for assessing tumor response to therapies including chemotherapy, molecular targeted agents, radiotherapy, and ablations [5, 6, 7•, 8–11]. More powerful post-processing software and techniques, including statistical and pure iterative reconstruction, permit radiation dose savings while maintaining or improving CT image quality. Iterative reconstruction has been proven to significantly improve CT image quality, predominantly in regard to noise reduction thereby facilitating moderate to marked radiation dose reduction, though altered image-texture may degrade diagnostic confidence [12].

In this review, we examine the recent literature pertaining to liver CT, including a range of technologies such as dual-energy CT and perfusion CT, low-tube-voltage techniques and post-processing techniques such as iterative reconstruction.

Dual-Energy CT of the Liver

Dual-energy CT was first conceptualized during the early development of CT, but was not clinically available until the first dual-source scanners, introduced in 2006, eliminated the problem of misregistration [13–16]. Recent advances in scanner technology have made the routine clinical use of DECT feasible. Several applications for liver imaging, predicated upon DECT's ability to differentiate materials based on their different X-ray attenuation coefficients at different photon energies, have been investigated, including improved detection of hypervascular and hypovascular liver lesions and the quantification of hepatic fat and iron [1, 2•, 17, 18•, 19, 20].

DECT acquires two image datasets of the same anatomy with two peak energies, 80- and 140-kVp, enabling structures of similar density but different elemental compositions, such as iodine, barium, or calcium, to be distinguished and iodine-levels potentially quantified, facilitating the determination of lesion enhancement [21, 22]. DECT can generate multiple datasets simultaneously, including material density maps, monochromatic images, and virtual unenhanced (VUE) images [23]. Material density maps assess the presence and amount of a particular element in an image such as iodine in a target lesion. This allows, for example, the potential differentiation of a small cyst and a poorly enhancing solid lesion.

CT manufacturers have taken different approaches to DECT, with scanner configurations that differ in their X-ray sources or detectors. These include dual-source scanning (SOMATOM Definition, Siemens Healthcare), with two orthogonal X-ray tubes generating 80 and 140 kVp X-ray spectra, respectively, single-source scanning with fast kilovoltage switching between 80 and 140 kVp at submillisecond intervals during a single gantry rotation (Discovery CT 750HD, GE Healthcare), single-source scanning acquiring spectral data through two consecutive scans at different kilovoltages (e.g., SOMATOM Definition AS/Edge, Siemens Healthcare), and single-source scanning using a spectral detector, that determines the energy levels of detected X-ray photons (IQon Spectral CT, Philips Healthcare).

Current limitations to the widespread adaptation of DECT include the high cost of such CT scanners, increased workflow complexity, and the lack of reimbursement for DECT above the level of conventional CT [24].

VUE Images

VUE images afford DECT the potential advantage of eliminating the need for a conventional unenhanced scan or obviating a follow-up dual-phase study to characterize an incidental lesion as non-enhancing, thereby saving radiation dose [25]. VUE images are generated by subtracting iodine from contrast-enhanced DECT images, based on the known behavior of iodine at different energies [26•]. However, the accuracy of the VUE attenuation values remains controversial since attenuation values may differ depending on the type of scanner, dynamic phase of images being evaluated, and the location of the region in question within the bore of the scanner [27]. For example, the dual-source approach creates VUE images in which Hounsfield units are available, the energy approach uses either two-material decomposition (water minus iodine), which does not provide Hounsfield units or a new technique, material suppression iodine (MSI), utilizing a three-material decomposition that does provide Hounsfield unit measurements.

De Cecco et al. examined VUE images of the liver and concluded that despite excellent subjective image quality, VUE cannot yet replace conventional unenhanced images in the clinical setting owing to limitations of the VUE images, including incomplete iodine subtraction, which could hamper the assessment of liver lesion enhancement, the erroneous subtraction of small calcifications, which can hinder lesion characterization, and significant differences in tissue density measurements between VUE and conventional unenhanced scans [17]. A further limitation of VUE is that pre-existing hyperdense material containing iodine, such as ethiodized oil used in chemoembolization (e.g., lipiodol), or iodinated GI contrast (Fig. 1), is also removed in the generation of VUE images [16]. This can potentially lead to the misinterpretation that a tumor that had been chemoembolized with lipiodol is "enhancing" when comparing VUE and post-contrast images [28].

Despite their limitations, VUE images can help narrow differential diagnoses by depicting foci of calcification (e.g., mucin-producing metastases or infectious/inflammatory lesions), fat (e.g., hepatocellular adenomas or HCC), or hemorrhage (e.g., adenomas) within liver lesions, which could be masked by iodinated contrast material [26•].

Gallstones and Bile Duct Stones

VUE images show moderate accuracy for detecting gallstones or bile duct stones and are a reasonable replacement for true unenhanced image sets (Fig. 2a, b). However, VUE images were noted to be particularly limited in detecting small gallstones measuring <9 mm^2 (Fig. 2c, d) or relatively radiolucent bile duct stones (<78 HU), failing to show stones in 16 % of evaluated patients [29].

Focal Liver Lesion Evaluation

DECT as well as low-tube-voltage techniques, described later in this review, may improve the conspicuity of liver

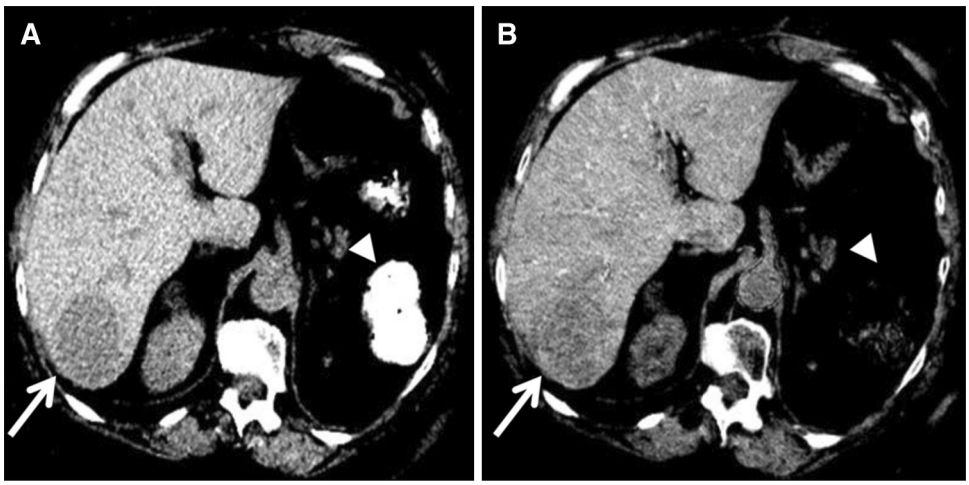

Fig. 1 Comparison of conventional unenhanced CT image to VUE image. Conventional unenhanced CT image **a** shows a hypodense metastasis (*arrow*) in the posterior right hepatic lobe. Hyperdense gastrointestinal contrast (*arrowhead*) is seen in the splenic flexure of the colon. VUE image **b** (water minus iodine material density image) shows the liver lesion (*arrow*), but it appears more heterogeneous and its borders less well defined, a limitation of the VUE image. Small opacified vessels remain visible in the liver on the VUE image due to incomplete iodine subtraction. Note that the iodinated GI contrast material in the splenic flexure of the colon (*arrowhead*) has been subtracted. If barium had been used for GI contrast, it would have remained visible

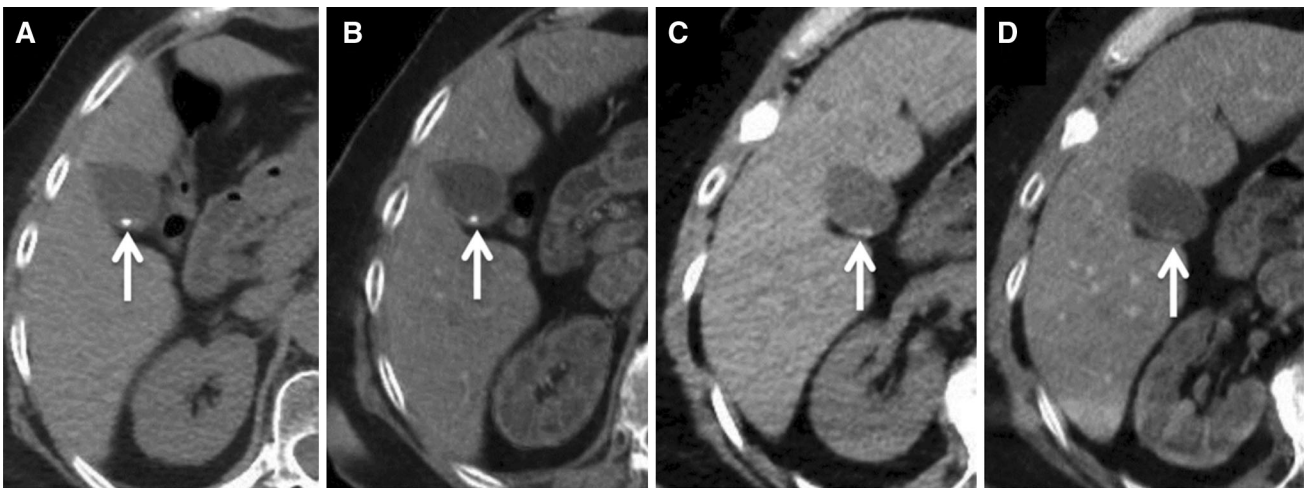

Fig. 2 Evaluation of gallstones on conventional unenhanced CT and VUE images. A small calcified gallstone (*arrow*) is well depicted on both the conventional unenhanced CT (**a**) and the VUE image (**b**). However, a few tiny layering gallstones (*arrow*) are poorly seen on the VUE image (**d**) compared to the conventional unenhanced CT (**c**). Very small gallstones and radiolucent bile duct stones can be missed on VUE images

lesions, especially hypervascular liver lesions. At low kV (80–100 kVp), iodinated contrast material demonstrates higher attenuation values owing to the proximity to the k-edge of iodine (33.2 keV) [30]. Low kV improves conspicuity of hypervascular liver lesions by increasing contrast between enhancing lesions and background liver, and therefore may improve lesion detection [18•, 31, 32]. Increased detection of hypovascular liver lesions can also be achieved on portal-venous phase imaging [4]. When DECT is performed in the portal-venous phase, 80-kVp data sets showed higher liver-to-lesion ratios with increased conspicuity of metastases compared to 120-kVp data sets, owing to the greater attenuation of iodine in enhancing liver parenchyma relative to hypoenhancing metastases at this tube voltage. Conversely, 80-kVp data sets have been shown to be more sensitive in the arterial phase for detecting hypervascular lesions [3].

In addition, DECT has the advantage of generating iodine density images or iodine maps that can display areas of tissue enhancement by detecting and potentially quantifying the amount of iodine within each voxel. This technique can detect even a small amount of enhancement

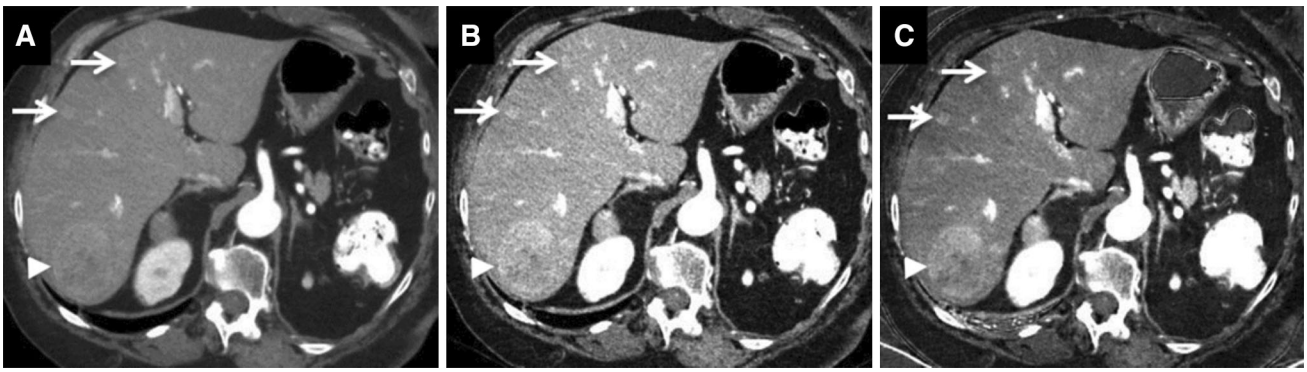

Fig. 3 DECT monochromatic 70- and 50-keV images and iodine material density image depicting neuroendocrine tumor metastases to the liver in a 66-year-old woman. Monochromatic 70-keV image **a** from contrast-enhanced DECT in the arterial phase shows a large hypervascular metastasis (*arrowhead*) in the posterior right hepatic lobe and two additional faint subcentimeter hypervascular metastases (*arrows*). Monochromatic 50-keV DECT image (**b**) and material-specific iodine image (iodine minus water) (**c**) show increased conspicuity of the smaller lesions (*arrows*) compared to the 70-keV image (**a**). Note the greater attenuation of iodinated contrast material in the 50-keV image (**b**) compared to the 70-keV image (**a**) at the same window width/level owing to the higher attenuation of iodine as the CT photon energies approach the k-edge of iodine.

within a lesion [25, 32, 33] and can be used as a potential surrogate to assess tumor vascularization as an imaging biomarker of tumor response to therapy [34, 35].

DECT polychromatic raw data can also be postprocessed to generate virtual monochromatic image sets at single voltages ranging from 40 to 140 keV usually in increments of 10 keV, which resemble an acquisition performed with X-rays of only that energy level [36]. The optimal monochromatic image set for evaluating various liver pathologies has been the subject of numerous recent studies. Shuman et al. compared various monochromatic image sets (40-, 50-, 70-, and 77-keV) for the detection of hypervascular lesions on the late arterial phase and determined that the greatest subjective lesion conspicuity and measured contrast-to-noise ratio was noted at 50 keV. The 50-keV images had a measured lesion CNR at least 70 % greater than the 77-keV images, and a few more lesions were seen at the lower monochromatic energies than at 77 keV, although the difference was not statistically significant [37•]. We have noted in our practice similar improvement in hypervascular lesion visualization and include 50-keV monochromatic images with our DECT images sets (Fig. 3).

Sudarski et al. evaluated multiple monochromatic image sets ranging from 40 to 120 keV of the portal-venous phase in the evaluation of hepatic metastases from GIST [36]. They found that 70-keV monochromatic images had the highest objective image quality, in terms of lowest image noise and highest liver and metastasis-to-liver CNRs, among the reconstructed data sets, but that the monochromatic images were not superior to the 120 kVp polychromatic images. Subjective image quality, on the other hand, was rated best for the 70-keV images [36]. Similarly, Yamada et al. found that 70-keV images performed best for evaluating hypovascular liver metastases, with lowest image noise for liver parenchyma and the highest CNR for hypovascular liver metastases [38].

In daily practice, it is not feasible or necessary to generate and review all possible monochromatic image sets for every patient. With the data from the aforementioned studies and future studies, it is plausible that DECT scanners can be configured to choose the optimal monochromatic image sets to send to the reading workstation based on the indication for the examination or history of cancer. At our institution, we generally primarily evaluate the 70-keV image sets and use the 50-keV and iodine material density images as supplemental sources of information.

Hepatic Steatosis

Nonalcoholic fatty liver disease, of which hepatic steatosis is an early form, can lead to liver fibrosis and cirrhosis and may accelerate the development of type 2 diabetes and cardiovascular disease [39]. Given the high and increasing prevalence of fatty liver disease, affecting about 20 % of the US adult population, the ability to determine liver fat content on routine post-contrast DECT performed for unrelated reasons without the need of a conventional unenhanced image set provides an opportunity to screen patients for steatosis, stratify risk, and minimize radiation exposure [27, 40]. On conventional unenhanced CT, a liver attenuation value of 48 HU or less has been shown to be 100 % specific for moderate to severe steatosis (≥30 % fat at histology) with a sensitivity of 54 % [41]. While conventional CT attenuation is presented in Hounsfield units, material density VUE images present parenchymal values in units of milligram per milliliter (mg/mL) of the material

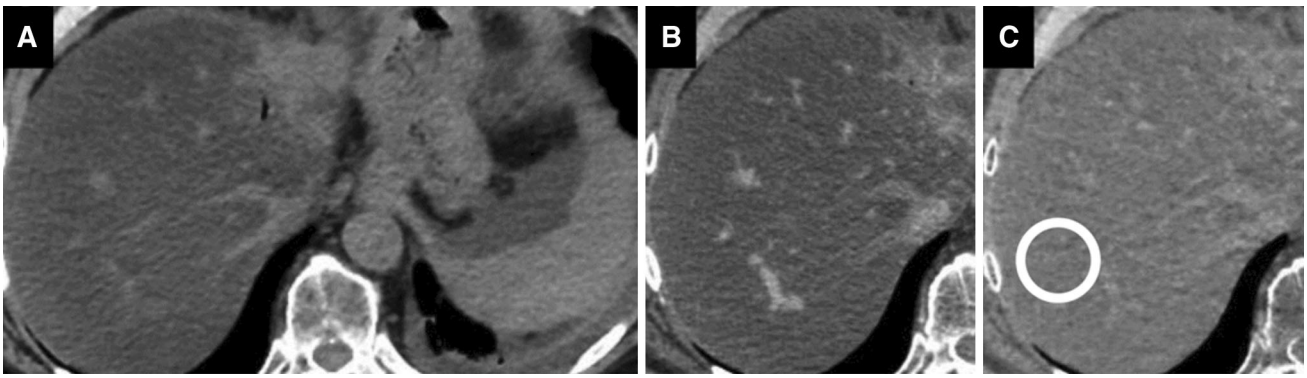

Fig. 4 Hepatic steatosis assessed with DECT. Conventional unenhanced CT image **a** shows hypoattenuating liver parenchyma that measured −8 HU in density, compatible with severe steatosis. 70-keV monochromatic image **b** generated from DECT shows enhancing vessels in the low density liver. VUE image **c** generated from the contrast-enhanced DECT with a simulated ROI (*circle*) that measured 986 mg/cc, below the 1027 mg/cc threshold for diagnosing steatosis on VUE images

being measured and thus cannot readily be used to estimate hepatic fat content on the basis of an accepted HU value.

Patel et al. recently validated VUE DECT images derived from contrast-enhanced rapid-switching DECT for liver fat quantification and determined that a liver region-of-interest drawn on the VUE images with a threshold of 1,027 mg/ml or below demonstrated a 90 % sensitivity and 61 % specificity for the presence of clinically relevant steatosis, without the need of a conventional unenhanced CT (Fig. 4) [1]. Recent animal studies have shown that DECT is comparable in accuracy to conventional unenhanced CT and MRI for quantifying liver fat [42–44], but may be more accurate in the presence of hepatic iron [45]. Fischer et al. showed, in an ex vivo animal study, that an iron-specific three-material decomposition algorithm can subtract iron and contrast media from the DECT data enabling accurate liver fat quantification, which would otherwise by underestimated in the presence of iron's confounding increase in liver attenuation [45].

Quantification of Liver Iron

A range of liver diseases, including alcoholic liver disease, chronic viral hepatitis, and nonalcoholic steatohepatitis, as well as long-term blood transfusions and hereditary hemochromatosis can lead to excessive iron deposition in hepatocytes, which can result in liver damage through iron-mediated oxidative stress [2•, 46, 47]. DECT has been shown to be accurate for diagnosing clinically significant (>10 %) hepatic iron accumulation with diagnostic performance similar to MRI [2•, 48]. Joe et al. assessed dual-source dual-energy CT and single-source dual-energy CT, both manufactured by Siemens, for analyzing the iron concentrations in liver phantoms and in liver transplant candidates, and compared the accuracy to MRI. The difference in liver attenuation (ΔH), measured in Hounsfield units, on unenhanced DECT performed at 80 and 140 kVp, was shown to be significantly higher in patients with ≥10 % hepatic iron accumulation ($\Delta H = 13.5$) compared to patients with <10 % hepatic iron accumulation ($\Delta H = 7.4$) (p value <0.001). DECT was thus able to differentiate these two patient groups using an optimal cutoff value for ΔH of 12.5 with a sensitivity of 80 % (8 of 10 patients) and a specificity of 90 % (69 of 77 patients) [2•]. A limitation of the study was that only a single manufacturer's DECT was evaluated and validation across other DECT platforms is needed. Since the assessment of iron with DECT is performed without IV contrast material, it cannot be applied to routine contrast-enhanced DECT. Further, the presence of significant hepatic steatosis may be a confounder when quantifying hepatic iron levels [2•]. Nevertheless, this study shows an exciting possibility for non-invasively evaluating hepatic iron overload, potentially obviating a biopsy, and could be especially useful in patients with a contraindication to MRI.

Perfusion CT of the Liver

Perfusion CT is a non-invasive functional imaging technique that quantitatively and qualitatively assesses perfusion in an organ based on the temporal changes in tissue attenuation after intravenous iodinated contrast material administration. Perfusion CT is routinely used in neuroimaging for the evaluation of acute ischemic stroke, but its use in the abdomen is relatively nascent, currently predominantly in the setting of clinical trials and research protocols.

Perfusion CT of the liver can be used to characterize and differentiate focal lesions, monitor treatment response and tumor recurrence following loco-regional and systemic therapies for metastatic or primary hepatic tumors, and

may be helpful in predicting response to therapy based on baseline tumor vascularity [5–11, 49]. Molecular-targeted therapies for treating cancer that target tumor vasculature can be cytostatic rather than cytotoxic. Their clinical effects can be underestimated using traditional imaging response assessment criteria such as Response Evaluation Criteria in Solid Tumors (RECIST) that evaluate solely changes in tumor size. Perfusion CT, in contradistinction, can assess changes in tumor vascularity in response to therapies and has gained traction as an early and potentially more accurate imaging biomarker of therapeutic response particularly in the setting of novel therapies [6].

Perfusion CT of the liver is performed by acquiring serial CT images in quick succession following intravenous-iodinated contrast material administration and enables the evaluation of dynamic changes in liver perfusion, tumor hemodynamics, and vessel attenuation. Several quantitative perfusion indices and maps can be derived including tissue blood volume (BV), blood flow (BF), mean transit time (MTT), and permeability-surface area product which can be calculated with various kinetic models [16]. An in depth discussion of the technical principles and protocols of perfusion CT is beyond the scope of this article but is summarized in the recent review article by Kim et al. [50•]. CT manufacturers each offer their own perfusion analysis software based on varied kinetic models, which can affect calculated perfusion parameters and thus may limit comparison of perfusion indices across CT platforms [51, 52]. Currently, there is no consensus on a scanning protocol or analysis model for liver perfusion CT [52].

Other limitations of perfusion CT include the risk of ionizing radiation, given the multiple sequential scans of the organ of interest, and degradation of CT data due to motion, specifically respiratory misregistration. The risk of ionizing radiation can be reduced by scanning at a lower tube current or voltage combined with newer iterative reconstruction techniques to maintain image quality [53]. A recent study showed that the choice of image reconstruction method does not adversely affect hepatic perfusion values either with or without radiation dose reductions [54]. Respiratory gating, motion-tracking software, and the use of new generation MDCT scanners with wider detector rows, currently spanning up to 16 cm of *z*-axis coverage, can minimize misregistration artifacts [7•]. Recent data show that even artifacts from free breathing can be negated with novel respiratory motion correction algorithms [55].

Perfusion CT in Hepatocellular Carcinoma

Hepatocellular carcinoma (HCC) is the sixth most common cancer worldwide and ranks third in cancer-related mortality [56]. The main risk factor for this tumor is liver cirrhosis from all causes, including chronic viral hepatitis (hepatitis C and B), alcohol, and nonalcoholic fatty liver disease.

Untreated HCC has a dismal prognosis with a median survival of 6 months after diagnosis [57]. Surgical resection is the treatment of choice for early-stage disease, however, only 20 % of patients are eligible for surgery at the time of diagnosis [57].

Hepatocarcinogenesis occurs in a multistep process, whose hallmark is the alteration in the relative arterial and portal venous BF of the nodule in a cirrhotic liver [16]. As a liver nodule progresses from a dysplastic nodule to a well-differentiated HCC and subsequently to moderately and poorly differentiated HCC, the relative arterial flow to the lesion increases, which can be assessed with perfusion CT (Fig. 5) [16]. CT perfusion changes can thus be used to detect HCC, act as an imaging biomarker to predict the level of tumor differentiation, and to monitor response to therapy (Fig. 6).

For unresectable large (>3 cm) HCCs, transcatheter arterial chemoembolization (TACE) is the primary treatment and consists of delivering chemotherapy locally with arterial embolization to destroy tumor cells [7•]. Radiofrequency ablation (RFA) is the best option for smaller (<3 cm) HCCs when there are three or fewer tumors and when surgical resection or liver transplantation is contraindicated [58]. Tumor recurrence following these therapies is common, with local recurrence as high as 61.8 % at 1 year following TACE [59], and early detection of residual or recurrent disease is critical for identifying sites needing retreatment.

Perfusion CT in Treatment Response Evaluation

Ippolito et al. investigated the possible influence of interventional treatments of HCC on perfusion values and demonstrated that perfusion CT is a robust and reproducible technique for evaluating tumor response to transarterial chemoembolization and RFA and was not degraded by imaging changes from these loco-regional therapies such as attenuation changes from tumor necrosis or iodized oil, that could confound assessment by conventional imaging features alone on MDCT [7•]. They found a significant difference ($p < 0.001$) for all perfusion parameters (hepatic perfusion, arterial perfusion, BV, time to peak, and hepatic perfusion index) between residual viable tumor and completely treated lesions, enabling their differentiation [7•].

Perfusion CT is well suited for the assessment of response following anti-angiogenic therapies since vascular changes can be assessed prior to tumor volume changes and viable tumor can be differentiated from necrotic or fibrotic tissue [52]. Jiang et al. demonstrated that CT

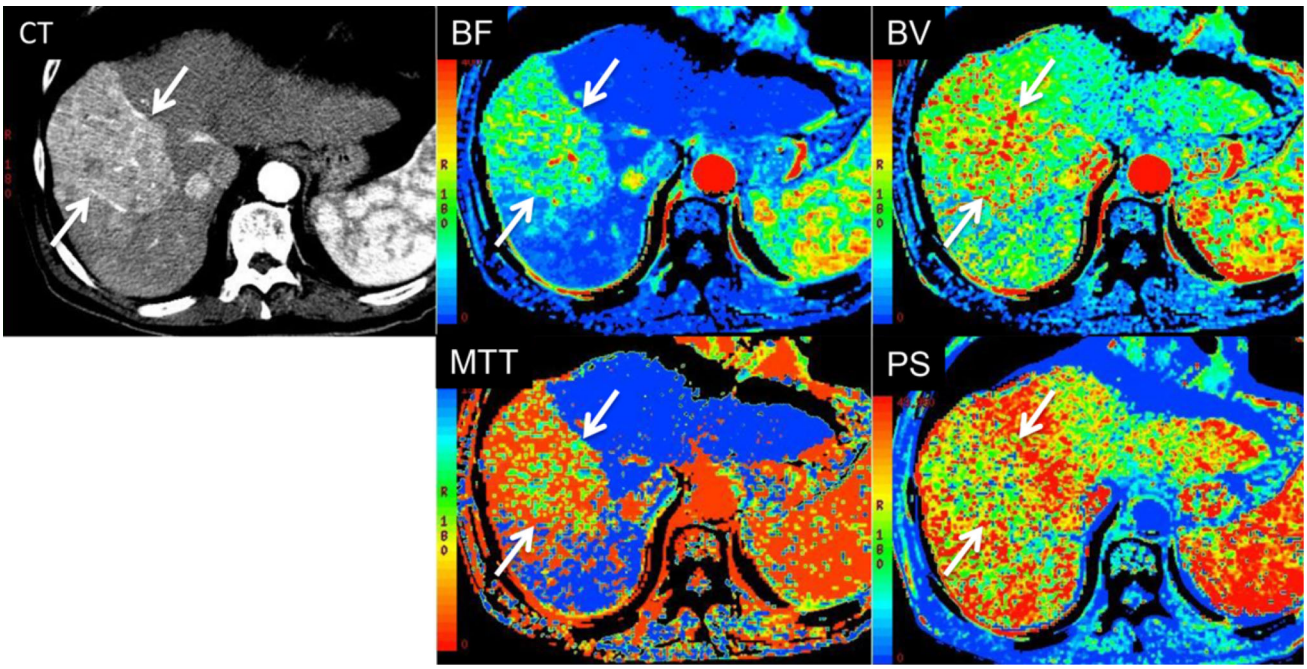

Fig. 5 Perfusion CT of HCC. Axial CECT (CT) and respective functional maps of blood flow (BF), blood volume (BV), mean transit time (MTT), and permeability surface area product (PS) in a 79-year-old with a large hypervascular HCC (*arrows*) in the right lobe of the liver. Perfusion values from regions of interest drawn around the tumor and representative surrounding normal liver parenchyma show BF of 132.3 and 5.4 mL/100 g/min, BV of 5.8 and 2.3 mL/100 g, MTT of 4.4 and 26.3 s, and PS of 32.5 and 25.1 mL/100 g/min, respectively. The higher perfusion parameters are indicative of the preferential arterial supply to HCC compared with the dual vascular supply to the normal liver parenchyma

perfusion is a more sensitive imaging biomarker for monitoring treatment changes and predicting progression-free survival in advanced HCC treated with antioangiogenic therapy (bevacizumab) compared to RECIST and tumor density measurements [49]. HCC with a higher baseline MTT correlated with a favorable clinical outcome [49].

Frampas et al. prospectively examined perfusion CT in a small cohort of patients with advanced HCC treated with targeted therapy (sorafenib and sunitinib) and compared it to dynamic contrast-enhanced ultrasound (DCE-US) at 1 month post therapy [60]. While perfusion measurements of both techniques were highly sensitive to targeted therapies, they found that perfusion CT could not discriminate progressors from non-progressors at 1 month post treatment, whereas DCE-US could, and suggested DCE-US be used as a biomarker to monitor treatment in HCC treated with targeted therapies [60]. These results would need validation in larger independent studies.

Sorafenib is currently the approved line of last treatment for advanced HCC [61]. In a small scale study, Sacco et al. showed a significant increase in MTT in HCC at 3 months after treatment with sorafenib compared to baseline and found that the baseline MTT had an inverse correlation with reduction in alpha-fetoprotein levels following treatment [61]. MTT may therefore have a role as a predictive biomarker of therapeutic response in HCC treated with sorafenib and may aid in selecting the optimal treatment strategy, although additional studies are needed to substantiate these initial findings [61].

In summary, perfusion CT is feasible for monitoring treatment response in advanced HCC treated with molecular targeted therapies and loco-regional therapies.

Perfusion CT in Metastatic Disease

Transarterial radioembolization with yttrium-90-labeled microspheres is a treatment option for patients with unresectable liver-dominant metastatic disease from a number of primary tumors. The arterial perfusion of hepatic metastases has been shown to be different between lesions that respond versus that do not respond to radioembolization and perfusion CT can be used to quantify the extent of arterial perfusion of metastatic lesions, enabling response prediction [8]. Morsbach et al. showed that perfusion CT is the best predictor of morphologic response to therapy and 1-year survival following radioembolization compared to imaging with ^{99m}Tc-MAA SPECT and routine multiphase CT [8]. Perfusion CT had a sensitivity of 91 % and specificity of 95 % for predicting short-term morphologic response to therapy [8]. A high degree of arterial perfusion

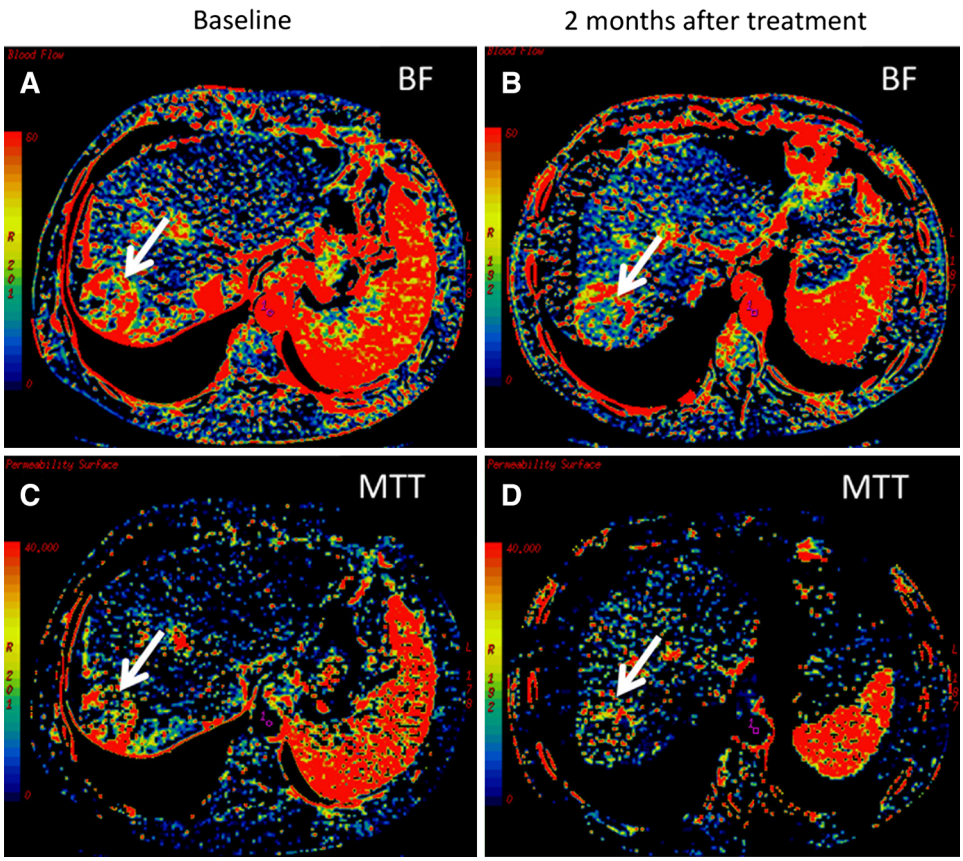

Fig. 6 Liver CT perfusion parameter maps in a patient with HCC in segment VII treated with the epidermal growth factor receptor (EGFR) inhibitor erlotinib. Blood flow (BF) and mean transit time (MTT) were significantly reduced at 2 months following treatment (**b**, **d**) compared to baseline (**a**, **c**), suggestive of response to treatment. The size of the HCC did not change significantly, which is a limitation for response criteria that evaluate solely changes in lesion size (e.g., RECIST)

of hepatic tumors prior to radioembolization was the single best predictor of 1-year survival following radioembolization, independent of hepatic tumor load [8].

Perfusion CT can also help distinguish HCCs from hypervascular metastases, which can appear similar on conventional CECT. Hayano et al. showed that the perfusion indices of BF, BV, and MTT of HCCs were substantially lower than those of hypervascular metastases, enabling differentiation [5]. ROC analysis demonstrated that of these perfusion parameters, tumor BV may be the most useful marker for differentiating between HCC and hypervascular metastases, with differential BV values postulated to result from increased microvascular resistance in HCC compared to metastases [5].

Radiation Dose-Reduction Techniques

The benefits of appropriately-used CT in patient care are indisputable. Over the past two decades, there has been a greater than threefold rise in the use of CT, with approximately 70 million scans performed annually in the US; medical imaging now contributes approximately 50 % of the overall radiation dose to the US population [62, 63]. Abdominal CT accounts for about a third of these CTs [64]. Although the incidence of cancer attributable to CT is difficult to estimate given the naturally high incidence of cancer in the population, the BEIR (Biological Effects of Ionizing Radiation) VII lifetime risk model estimates that 1 person in a 1000 would be expected to develop cancer from a dose of 10 mSv exposure above background [65]. The typical effective dose of an abdominal CT is 8 mSv but has a wide range based on individual technical and patient factors [66]. Given the widespread use of CT, it is crucial to use the ALARA (as low as reasonably achievable) concept to reduce any unnecessary radiation dose. Numerous recent articles have addressed radiation dose-reduction techniques in liver CT, including low voltage imaging and post-processing CT image noise reduction techniques.

Low-Tube-Voltage Liver CT

Several studies have shown that the visualization of hypervascular lesions in the liver can be improved by low-tube-voltage CT (80 or 100 kVp) compared to routine 120 or 140 kVp CT imaging when concomitant noise reduction techniques are used, while simultaneously reducing radiation dose [18•, 67–71]. The lower kVp generates X-rays that are closer in energy level to the *k*-edge of iodine (33.2 keV) resulting in greater attenuation of iodine from

an increase in the photoelectric effect and, therefore, greater conspicuity of iodinated contrast material [72].

Lower kVp imaging also leads to significant potential radiation dose reduction since radiation dose is directly related to the square of the kV. Therefore, lowering the kVp from 120 to 100 kVp or 120 to 80 kVp results in a dose reduction of approximately 33 and 65 %, respectively, when the tube current is held constant [72]. The major drawback of lower kVp imaging is decreased tissue penetration by lower-energy photons leading to higher image noise, which limits this technique to thinner adults, whose body-mass index (BMI) is under 25, and beam hardening with a potentially lower contrast-to-noise ratio (CNR) unless images noise is reduced [70]. Noise reduction can be achieved by increasing the tube current–time product (mAs), which has become more readily achievable with the introduction of very high output MDCT X-ray tubes that can generate high tube current peaks, with the latest scanners generating greater than 1,000 mA, and/or by using iterative reconstruction to process the CT data and thereby decrease noise [69]. A further limitation of low-kVp imaging is greater susceptibility to beam-hardening artifacts from high-density structures such as bone or dense contrast.

A number of recent studies have examined low-kVp liver CT coupled with various reconstruction techniques and generally found diagnostic improvement with the low-kVp imaging in thin patients [68, 73–76]. Yu et al. compared the image quality and detectability of hypervascular HCC using half-dose (300 mAs) 80-kVp liver CT with high level sinogram-affirmed iterative reconstruction (SAFIRE) versus virtual full-dose (600 mAs) 80-kVp scans reconstructed with filtered back projection (FBP). They found that the 80-kVp imaging with SAFIRE technique had image quality equivalent to or better than the full-dose 80-kVp FBP reconstructed images and also had a similar lesion-to-liver CNR for hyperenhancing HCCs [76]. The altered CT texture of the SAFIRE images described as having a "pixilated" appearance did not significantly influence diagnostic acceptability.

Hur et al. evaluated the conspicuity of hypervascular HCCs in patients and phantoms scanned in the late arterial phase with low-tube-voltage (80 kVp), intermediate tube current (340 mAs) with Iterative Reconstruction in Image Space (IRIS) versus standard 120 kVp CT with FBP algorithm [68]. Their data showed that in thin patients (mean BMI = 24 kg/m^2), small or subtly enhancing HCCs were more conspicuous on the low-tube-voltage CT reconstructed with IRIS compared to the standard 120 kVp imaging. When CNR was held constant, the low-kVp imaging resulted in a 41–84 % decrease in effective dose compared with 120 kVp scanning.

Namimoto et al. demonstrated improvement of liver image quality in 25 patients (mean BMI = 22.4 kg/m^2) at all three phases of enhancement (arterial, portal venous, and equilibrium) at lower radiation dose (9.0 vs 12.7 mGy) using a low-tube-voltage of 80 kVp with iterative reconstruction compared to 120-kVp imaging with FBP reconstruction. Additionally, they found better contrast enhancement of HCC despite reducing the iodinated contrast material by 25 % from 600 mg/kg (34.3 g of iodine) to 450 mg/kg (25.7 g of iodine), which can be of benefit in patients with borderline low renal function [77].

Although CT radiation dose reduction may be less critical in patients with malignancies that significantly reduce life expectancy, given the latency of radiation-induced tumor genesis, these techniques should be considered in young patients with chronic liver disease or in those with long-term disease-free survival, and who are undergoing multiple routine surveillance scans. Despite recent literature endorsing low-kVp imaging, it should be emphasized that this technique works best for thin or small patients and may not be appropriate in larger, overweight patients, owing to the excessive noise and decrease in image contrast in heavier patients due to photon deficiency and beam hardening. The technique may also be suboptimal in patients for whom CT image quality is paramount, such as in pre-surgical candidates where detail regarding small structures, such as vessels, may be necessary. Further studies are needed to determine the optimal tube voltages and currents that yield a balance between image quality and radiation dose for individual patient sizes and imaging indications.

Iterative Reconstruction Techniques

Numerous recent studies have examined and validated the use of diverse CT iterative reconstruction (IR) techniques from various vendors in liver CT, finding them to improve image quality (Fig. 7) and lesion detectability (Fig. 8) at similar or lower radiation dose compared to FBP. These studies have verified that the CT attenuation measurements, when placing a region-of-interest, are reproducible and do not change significantly between the various post-processing algorithms thus enabling evaluation of fatty liver or focal liver lesion density changes irrespective of the reconstruction technique [78, 79].

Yasaka et al. specifically examined the diagnosis of hepatic steatosis on CTs reconstructed using model-based IR (MBIR) versus FBP and determined that 120 kVp dose-reduced CT (mean CTDIvol of 1.91 mGy) with MBIR was comparable to routine dose 120 kVp CT (mean CTDIvol of 8.16 mGy) reconstructed with FBP using the diagnostic criteria of liver density <48 HU and a liver:spleen density ratio of <1.1 for diagnosing steatosis [78].

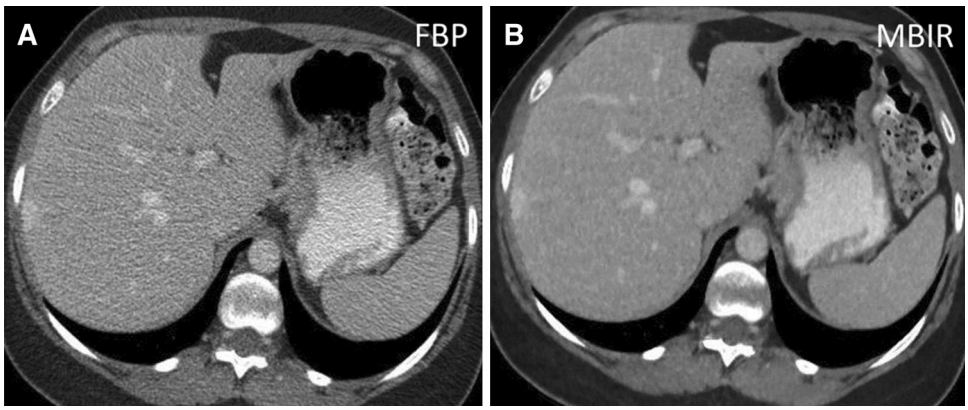

Fig. 7 Image noise reduction with model-based iterative reconstruction (MBIR). Axial CECT image reconstructed using FBP **a** shows a moderate amount of image noise. MBIR image **b** reconstructed from the same CT raw data shows a significant decrease in noise with improved delineation of hepatic vessels

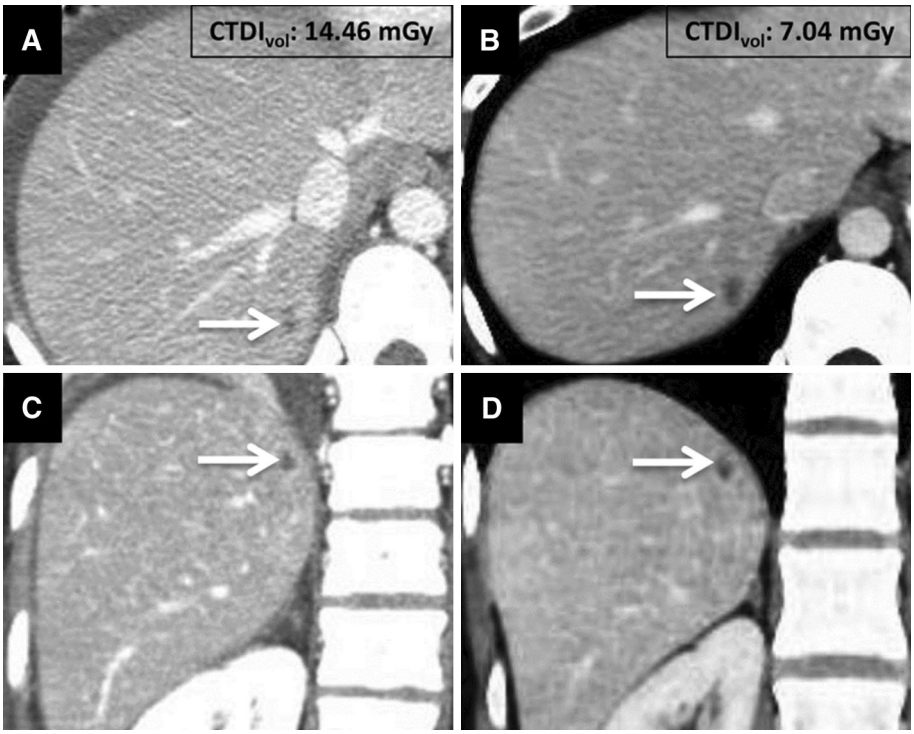

Fig. 8 Improved lesion conspicuity with IR despite a decrease in the CT radiation dose. Axial (**a**) and coronal (**c**) CECT images reconstructed with FBP show a small hypoattenuating lesion (*arrow*) in segment VII of the liver. The CTDIvol for the study was 14.46 mGy. Follow-up axial (**b**) and coronal (**d**) CECT images reconstructed using level 50 % of ASIR (GE Healthcare) show the same lesion. The CTDIvol for the followup study (7.04 mGy) was just under half the radiation dose of the initial study. Note the preservation in diagnostic accuracy of the images, despite a lower radiation dose, when using IR. Also note the different image texture in the IR images compared to FBP

In the evaluation of metastatic disease to the liver, newer reconstruction techniques have been shown to be superior in image quality and lesion detectability despite radiation dose reduction. Volders et al. compared the image quality of MBIR to that of 50 % adaptive statistical iterative reconstruction (ASIR) technique for detecting colorectal liver metastases on CT performed at 100 kVp. They determined that small metastases (<10 mm) were significantly better detected with MBIR than with ASIR despite scanning with a lower radiation dose of a mean $CTDI_{vol}$ of 5.18 mGy for the MBIR technique compared to a mean $CTDI_{vol}$ of 7.54 mGy for the ASIR technique. For lesions larger than 10 mm, they found no significant difference in lesion detection between the two reconstruction techniques as the larger lesions were well seen regardless of the noise level [80].

Conclusion

CT remains a critical tool in the evaluation of liver disease, despite competing advances in ultrasound and MRI. At this juncture, DECT offers some improvements in liver CT for the detection of focal lesions as well as several unique features for CT, such as quantifying hepatic iron or evaluating tumor iodine-enhancement without the need for pre-contrast images. We anticipate that the applicability of perfusion CT and DECT will continue to expand as the clinical paradigm

further shifts from anatomic imaging to include more functional liver imaging. Prospective research will be necessary to fully determine the validity of these modalities for imaging response biomarkers in oncology.

With the increasing emphasis on radiation dose reduction, low-kVp imaging and other dose-reduction methods coupled with newer iterative reconstruction techniques will continue to gain ground and wider use. Future studies should bring a better understanding of how far radiation dose can be reduced without compromising diagnostic acceptability for various imaging indications.

Compliance with Ethics Guidelines

Conflict of Interest Dr. Nicolaus A. Wagner-Bartak, Dr. Aran M. Toshav, Dr. Eric P. Tamm, Dr. Ott Le, Dr. Sheela Agarwal, Dr. Chaan Ng, and Dr. Aliya Qayyum each declare no potential conflicts of interest.

Human and Animal Rights and Informed Consent This article does not contain any studies with human or animal subjects performed by any of the authors.

References

Papers of particular interest, published recently, have been highlighted as:

- Of importance

1. Patel BN, Kumbla RA, Berland LL, Fineberg NS, Morgan DE. Material density hepatic steatosis quantification on intravenous contrast-enhanced rapid kilovolt (peak)-switching single-source dual-energy computed tomography. J Comput Assist Tomogr. 2013;37:904–10.
2. • Joe E, Kim SH, Lee KB, et al. Feasibility and accuracy of dual-source dual-energy CT for noninvasive determination of hepatic iron accumulation. Radiology. 2012; 262:126–35. *This study evaluated DECT for quantifying hepatic iron accumulation and showed that DECT performed on par with MRI.*
3. Altenbernd J, Heusner T, Ringelstein A, Ladd S, Forsting M, Antoch G. Dual-energy-CT of hypervascular liver lesions in patients with HCC: investigation of image quality and sensitivity. Eur Radiol. 2011;21:738–43.
4. Robinson E, Babb J, Chandarana H, MacAri M. Dual source dual energy MDCT: comparison of 80 kVp and weighted average 120 kVp data for conspicuity of hypo-vascular liver metastases. Invest Radiol. 2010;45:413–8.
5. Hayano K, Desai GS, Kambadakone AR, Fuentes JM, Tanabe KK, Sahani DV. Quantitative characterization of hepatocellular carcinoma and metastatic liver tumor by CT perfusion. Cancer Imaging. 2013;13:512–9.
6. Goh V, Ng QS, Miles K. Computed tomography perfusion imaging for therapeutic assessment: has it come of age as a biomarker in oncology? Invest Radiol. 2012;47:2–4.
7. • Ippolito D, Fior D, Bonaffini PA, et al. Quantitative evaluation of CT-perfusion map as indicator of tumor response to transarterial chemoembolization and radiofrequency ablation in HCC patients. Eur J Radiol. 2014; 83:1665–71. *This study showed that perfusion CT is a reproducible quantitative technique for the evaluation of treatment response of HCC following TACE and RFA.*
8. Morsbach F, Sah BR, Spring L, et al. Perfusion CT best predicts outcome after radioembolization of liver metastases: a comparison of radionuclide and CT imaging techniques. Eur Radiol. 2014;24:1455–65.
9. Reiner CS, Morsbach F, Sah BR, et al. Early treatment response evaluation after yttrium-90 radioembolization of liver malignancy with CT perfusion. J Vasc Interv Radiol. 2014;25:747–59.
10. Hao XJ, Li JP, Jiang HJ, et al. CT assessment of liver hemodynamics in patients with hepatocellular carcinoma after argon–helium cryoablation. Hepatob Pancreat Dis. 2013;12:617–21.
11. Morsbach F, Pfammatter T, Reiner CS, et al. Computed tomographic perfusion imaging for the prediction of response and survival to transarterial radioembolization of liver metastases. Invest Radiol. 2013;48:787–94.
12. Kordolaimi SD, Argentos S, Pantos I, Kelekis NL, Efstathopoulos EP. A new era in computed tomographic dose optimization: the impact of iterative reconstruction on image quality and radiation dose. J Comput Assist Tomogr. 2013;37:924–31.
13. Alvarez RE, Macovski A. Energy-selective reconstructions in X-ray computerized tomography. Phys Med Biol. 1976;21:733–44.
14. Kalender WA, Perman WH, Vetter JR, Klotz E. Evaluation of a prototype dual-energy computed tomographic apparatus I. Phantom studies. Med Phys. 1986;13:334–9.
15. Kaza RK, Platt JF, Cohan RH, Caoili EM, Al-Hawary MM, Wasnik A. Dual-energy CT with single- and dual-source scanners: current applications in evaluating the genitourinary tract. Radiographics. 2012;32:353–69.
16. Lee JM, Yoon JH, Joo I, Woo HS. Recent advances in CT and MR imaging for evaluation of hepatocellular carcinoma. Liver Cancer. 2012;1:22–40.
17. De Cecco CN, Darnell A, Macias N, et al. Virtual unenhanced images of the abdomen with second-generation dual-source dual-energy computed tomography: image quality and liver lesion detection. Invest Radiol. 2013;48:1–9.
18. • Marin D, Nelson RC, Samei E, et al. Hypervascular liver tumors: low tube voltage, high tube current multidetector CT during late hepatic arterial phase for detection–initial clinical experience. Radiology. 2009; 251:771–79. *Low tube voltage (80 kVp), high tube current CT was shown to increase the conspicuity of malignant hypervascular liver tumors compared to standard 140 kVp CT, while reducing radiation dose.*
19. Fletcher JG, Takahashi N, Hartman R, et al. Dual-energy and dual-source CT: is there a role in the abdomen and pelvis? Radiol Clin North Am. 2009;47:41–57.
20. Johnson TR, Krauss B, Sedlmair M, et al. Material differentiation by dual energy CT: initial experience. Eur Radiol. 2007;17: 1510–7.
21. Graser A, Johnson TR, Bader M, et al. Dual energy CT characterization of urinary calculi: initial in vitro and clinical experience. Invest Radiol. 2008;43:112–9.
22. Sahni VA, Shinagare AB, Silverman SG. Virtual unenhanced CT images acquired from dual-energy CT urography: accuracy of attenuation values and variation with contrast material phase. Clin Radiol. 2013;68:264–71.
23. De Cecco CN, Darnell A, Rengo M, et al. Dual-energy CT: oncologic applications. AJR Am J Roentgenol. 2012;199:S98–105.
24. Megibow AJ, Chandarana H, Hindman NM. Increasing the precision of CT measurements with dual-energy scanning. Radiology. 2014;272:618–21.
25. Heye T, Nelson RC, Ho LM, Marin D, Boll DT. Dual-energy CT applications in the abdomen. AJR Am J Roentgenol. 2012;199: S64–70.
26. • Agrawal MD, Pinho DF, Kulkarni NM, Hahn PF, Guimaraes AR, Sahani DV. Oncologic applications of dual-energy CT in the

abdomen. Radiographics. 2014; 34:589–612. *This review article discusses the principles of DECT including the utility of post-processed image sets. The role of DECT for lesion characterization and oncologic treatment planning and monitoring is reviewed.*
27. Morgan DE. Dual-energy CT of the abdomen. Abdom Imaging. 2014;39:108–34.
28. Barrett T, Bowden DJ, Shaida N, et al. Virtual unenhanced second generation dual-source CT of the liver: is it time to discard the conventional unenhanced phase? Eur J Radiol. 2012;81: 1438–45.
29. Kim JE, Lee JM, Baek JH, Han JK, Choi BI. Initial assessment of dual-energy CT in patients with gallstones or bile duct stones: can virtual nonenhanced images replace true nonenhanced images? AJR Am J Roentgenol. 2012;198:817–24.
30. Yeh BM, Shepherd JA, Wang ZJ, Teh HS, Hartman RP, Prevrhal S. Dual-energy and low-kVp CT in the abdomen. AJR Am J Roentgenol. 2009;193:47–54.
31. Schindera ST, Nelson RC, Mukundan S Jr, et al. Hypervascular liver tumors: low tube voltage, high tube current multi-detector row CT for enhanced detection—phantom study. Radiology. 2008;246:125–32.
32. Agrawal MD, Agarwal S, Fuentes-Oreego JM, Hayano K, Sahani DV. New liver imaging techniques. Curr Radiol Rep. 2013;1: 294–306.
33. Graser A, Johnson TR, Chandarana H, Macari M. Dual energy CT: preliminary observations and potential clinical applications in the abdomen. Eur Radiol. 2009;19:13–23.
34. Meyer M, Hohenberger P, Apfaltrer P, et al. CT-based response assessment of advanced gastrointestinal stromal tumor: dual energy CT provides a more predictive imaging biomarker of clinical benefit than RECIST or Choi criteria. Eur J Radiol. 2013;82: 923–8.
35. Apfaltrer P, Meyer M, Meier C, et al. Contrast-enhanced dual-energy CT of gastrointestinal stromal tumors: is iodine-related attenuation a potential indicator of tumor response? Invest Radiol. 2012;47:65–70.
36. Sudarski S, Apfaltrer P, Nance JW Jr, et al. Objective and subjective image quality of liver parenchyma and hepatic metastases with virtual monoenergetic dual-source dual-energy CT reconstructions: an analysis in patients with gastrointestinal stromal tumor. Acad Radiol. 2014;21:514–22.
37. • Shuman WP, Green DE, Busey JM, et al. Dual-energy liver CT: effect of monochromatic imaging on lesion detection, conspicuity, and contrast-to-noise ratio of hypervascular lesions on late arterial phase. AJR Am J Roentgenol. 2014; 203:601–6. *This prospective study assessed the optimal DECT monochromatic image set for the evaluation of hyperenhancing liver lesions in the arterial phase. The results showed the greatest subjective lesion conspicuity and highest CNR at 50 keV, but without a statistically significant increase in lesions detected compared to the 77-keV images.*
38. Yamada Y, Jinzaki M, Tanami Y, Abe T, Kuribayashi S. Virtual monochromatic spectral imaging for the evaluation of hypovascular hepatic metastases: the optimal monochromatic level with fast kilovoltage switching dual-energy computed tomography. Invest Radiol. 2012;47:292–8.
39. Targher G, Day CP, Bonora E. Risk of cardiovascular disease in patients with nonalcoholic fatty liver disease. New Engl J Med. 2010;363:1341–50.
40. Lazo M, Hernaez R, Eberhardt MS, et al. Prevalence of nonalcoholic fatty liver disease in the United States: the Third National Health and Nutrition Examination Survey, 1988–1994. Am J Epidemiol. 2013;178:38–45.
41. Pickhardt PJ, Park SH, Hahn L, Lee S-G, Bae KT, Yu ES. Specificity of unenhanced CT for non-invasive diagnosis of hepatic steatosis: implications for the investigation of the natural history of incidental steatosis. Eur Radiol. 2012;22:1075–82.
42. Hur BY, Lee JM, Hyunsik W, et al. Quantification of the fat fraction in the liver using dual-energy computed tomography and multi-material decomposition. J Comput Assist Tomogr. 2014;38(6): 845–52.
43. Sun T, Lin X, Chen K. Evaluation of hepatic steatosis using dual-energy CT with MR comparison. Front Biosci. 2014;19:1377.
44. Artz NS, Hines CD, Brunner ST, et al. Quantification of hepatic steatosis with dual-energy computed tomography: comparison with tissue reference standards and quantitative magnetic resonance imaging in the ob/ob mouse. Invest Radiol. 2012;47:603.
45. Fischer MA, Gnannt R, Raptis D, et al. Quantification of liver fat in the presence of iron and iodine: an ex vivo dual-energy CT study. Invest Radiol. 2011;46:351–8. doi:10.1097/RLI.1090b1013e31820e31486.
46. Ramm GA, Ruddell RG. Hepatotoxicity of iron overload: mechanisms of iron-induced hepatic fibrogenesis. Semin Liver Dis. 2005;25:433–49.
47. Alla V, Bonkovsky HL. Iron in nonhemochromatotic liver disorders. Semin Liver Dis. 2005;25:461–72.
48. Tsai YS, Chen JS, Wang CK, et al. Quantitative assessment of iron in heart and liver phantoms using dual-energy computed tomography. Exp Ther Med. 2014;8:907–12.
49. Jiang T, Kambadakone A, Kulkarni NM, Zhu AX, Sahani DV. Monitoring response to antiangiogenic treatment and predicting outcomes in advanced hepatocellular carcinoma using image biomarkers, CT perfusion, tumor density, and tumor size (RECIST). Invest Radiol. 2012;47:11–7.
50. • Kim SH, Kamaya A, Willmann JK. CT perfusion of the liver: principles and applications in oncology. Radiology. 2014; 272:322–44. *A comprehensive review article that discusses perfusion CT of the liver in oncology. Technical details of perfusion imaging including the various analytic methods and models for calculating perfusion indices are described. The article elaborates upon the role of perfusion CT for the early detection of liver tumors, assessment of prognosis, monitoring of therapy, and the diagnosis of tumor recurrence.*
51. Lee JM, Yoon J-H, Kim KW. Diagnosis of hepatocellular carcinoma: newer radiological tools. Semin Oncol. 2012;39:399–409.
52. Hayano K, Fuentes-Orrego JM, Sahani DV. New approaches for precise response evaluation in hepatocellular carcinoma. World J Gastroenterol. 2014;20:3059–68.
53. Ogul H, Kantarci M, Genc B, et al. Perfusion CT imaging of the liver: review of clinical applications. Diagn Interv Radiol. 2014; 20:379–89.
54. Negi N, Yoshikawa T, Ohno Y, et al. Hepatic CT perfusion measurements: a feasibility study for radiation dose reduction using new image reconstruction method. Eur J Radiol. 2012;81: 3048–54.
55. Jensen NK, Lock M, Fisher B, et al. Prediction and reduction of motion artifacts in free-breathing dynamic contrast enhanced CT perfusion imaging of primary and metastatic intrahepatic tumors. Acad Radiol. 2013;20:414–22.
56. Ferlay J, Shin HR, Bray F, Forman D, Mathers C, Parkin DM. Estimates of worldwide burden of cancer in 2008: GLOBOCAN 2008. Int J Cancer. 2010;127:2893–917.
57. Ramsey DE, Kernagis LY, Soulen MC, Geschwind JF. Chemoembolization of hepatocellular carcinoma. J Vasc Interv Radiol. 2002;13:S211–21.
58. Shiina S, Tateishi R, Arano T, et al. Radiofrequency ablation for hepatocellular carcinoma: 10-year outcome and prognostic factors. Am J Gastroenterol. 2012;107:569–77.
59. Kinugasa H, Nouso K, Takeuchi Y, et al. Risk factors for recurrence after transarterial chemoembolization for early-stage hepatocellular carcinoma. J Gastroenterol. 2012;47:421–6.

60. Frampas E, Lassau N, Zappa M, Vullierme MP, Koscielny S, Vilgrain V. Advanced hepatocellular carcinoma: early evaluation of response to targeted therapy and prognostic value of perfusion CT and dynamic contrast enhanced-ultrasound. Preliminary results. Eur J Radiol. 2013;82:e205–11.
61. Sacco R, Faggioni L, Bargellini I, et al. Assessment of response to sorafenib in advanced hepatocellular carcinoma using perfusion computed tomography: results of a pilot study. Dig Liver Dis. 2013;45:776–81.
62. de Berrington Gonzalez A, Mahesh M, Kim KP, et al. Projected cancer risks from computed tomographic scans performed in the United States in 2007. Arch Intern Med. 2009;169:2071–7.
63. Mettler FA Jr, Bhargavan M, Faulkner K, et al. Radiologic and nuclear medicine studies in the United States and worldwide: frequency, radiation dose, and comparison with other radiation sources–1950-2007. Radiology. 2009;253:520–31.
64. Maldjian PD, Goldman AR. Reducing radiation dose in body CT: a primer on dose metrics and key CT technical parameters. AJR Am J Roentgenol. 2013;200:741–7.
65. National Research Council, Committee on Health Effects of Exposure to Low Levels of Ionizing Radiations (BEIR VII). Health effects of exposure to low levels of ionizing radiations: time for reassessment? Washington DC: National Academy Press; 1998.
66. Mettler FA, Huda W, Yoshizumi TT, Mahesh M. Effective doses in radiology and diagnostic nuclear medicine: a catalog. Radiology. 2008;248:254–63.
67. Ehman EC, Guimaraes LS, Fidler JL, et al. Noise reduction to decrease radiation dose and improve conspicuity of hepatic lesions at contrast-enhanced 80-kV hepatic CT using projection space denoising. AJR Am J Roentgenol. 2012;198:405–11.
68. Hur S, Lee JM, Kim SJ, Park JH, Han JK, Choi BI. 80-kVp CT using Iterative Reconstruction in Image Space algorithm for the detection of hypervascular hepatocellular carcinoma: phantom and initial clinical experience. Korean J Radiol. 2012;13:152–64.
69. Marin D, Nelson RC, Schindera ST, et al. Low-tube-voltage, high-tube-current multidetector abdominal CT: improved image quality and decreased radiation dose with adaptive statistical iterative reconstruction algorithm–initial clinical experience. Radiology. 2010;254:145–53.
70. Lee KH, Lee JM, Moon SK, et al. Attenuation-based automatic tube voltage selection and tube current modulation for dose reduction at contrast-enhanced liver CT. Radiology. 2012;265:437–47.
71. Park JH, Kim SH, Park HS, et al. Added value of 80 kVp images to averaged 120 kVp images in the detection of hepatocellular carcinomas in liver transplantation candidates using dual-source dual-energy MDCT: results of JAFROC analysis. Eur J Radiol. 2011;80:e76–85.
72. Raman SP, Johnson PT, Deshmukh S, Mahesh M, Grant KL, Fishman EK. CT dose reduction applications: available tools on the latest generation of CT scanners. J Am Coll Radiol. 2013;10:37–41.
73. Hur BY, Lee JM, Joo I, et al. Liver computed tomography with low tube voltage and model-based iterative reconstruction algorithm for hepatic vessel evaluation in living liver donor candidates. J Comput Assist Tomogr. 2014;38:367–75.
74. Marin D, Choudhury KR, Gupta RT, et al. Clinical impact of an adaptive statistical iterative reconstruction algorithm for detection of hypervascular liver tumours using a low tube voltage, high tube current MDCT technique. Eur Radiol. 2013;23:3325–35.
75. Husarik DB, Schindera ST, Morsbach F, et al. Combining automated attenuation-based tube voltage selection and iterative reconstruction: a liver phantom study. Eur Radiol. 2014;24:657–67.
76. Yu MH, Lee JM, Yoon JH, et al. Low tube voltage intermediate tube current liver MDCT: sinogram-affirmed iterative reconstruction algorithm for detection of hypervascular hepatocellular carcinoma. AJR Am J Roentgenol. 2013;201:23–32.
77. Namimoto T, Oda S, Utsunomiya D, et al. Improvement of image quality at low-radiation dose and low-contrast material dose abdominal CT in patients with cirrhosis: intraindividual comparison of low tube voltage with iterative reconstruction algorithm and standard tube voltage. J Comput Assist Tomogr. 2012;36:495–501.
78. Yasaka K, Katsura M, Akahane M, Sato J, Matsuda I, Ohtomo K. Dose-reduced CT with model-based iterative reconstruction in evaluations of hepatic steatosis: how low can we go? Eur J Radiol. 2014;83:1063–8.
79. Vardhanabhuti V, Loader RJ, Mitchell GR, Riordan RD, Roobottom CA. Image quality assessment of standard- and low-dose chest CT using filtered back projection, adaptive statistical iterative reconstruction, and novel model-based iterative reconstruction algorithms. AJR Am J Roentgenol. 2013;200:545–52.
80. Volders D, Bols A, Haspeslagh M, Coenegrachts K. Model-based iterative reconstruction and adaptive statistical iterative reconstruction techniques in abdominal CT: comparison of image quality in the detection of colorectal liver metastases. Radiology. 2013;269:469–74.